ELSEVIER

Thermochimica Acta 384 (2002) 261–277

thermochimica acta

www.elsevier.com/locate/tca

Combustion of damaged PBX 9501 explosive

H.L. Berghout[1], S.F. Son[*], C.B. Skidmore, D.J. Idar, B.W. Asay

High Explosives Sci. & Tech group, Los Alamos National Laboratory, MS C920, Los Alamos, Los Alamos, NM 87545, USA

Abstract

Impact or thermal ignition of high explosives (HE) results in deformation that can lead to damage. Fractures or defects, combined with sufficient pressure, dramatically increase the available surface area and potentially changes even the mode of combustion. Recent impact and cookoff experiments on PBX 9501, (HMX, octahydro-1,3,5,7-tetranitro-1,3,5,7-tetrazocine, with a plasticized, Estane-based binder), have shown complex cracking patterns caused by impact or pressurization. Fast reactive waves have been observed to propagate through the cracks at hundreds of meters per second. We present experiments that examine the combustion of mechanically and thermally damaged samples of PBX 9501. Mechanically damaged samples, damaged by quasi-static compression, exhibit large, ~200 μm stress fracture accompanied by extensive rubblization. Combustion experiments determine a 1.4 ± 0.6 MPa critical pressure for the onset of violent convective combustion, consistent with connected porosity of 25 μm. Thermally damaged samples, damaged by heating in a 180 °C oven for 30 min, exhibit 2–20 μm cracks distributed throughout the sample. Combustion experiments indicate a 9.2 ± 0.4 MPa critical pressure for the onset of violent convective combustion in the thermally damaged sample, consistent with connected porosity of 4 μm. Below the critical pressure, the burn rate and pressure exponent of thermally damaged PBX 9501 are close to those of the pristine material.

Keywords: PBX 9501; Combustion; Cracking; Explosives; HMX

1. Introduction

The shift from conductive or normal burning to convective burning is an important step in the deflagration-to-detonation transition in explosives and other energetic materials [1–3]. Normal deflagration involves primarily conductive heat transfer from the gas-phase flame region to the surface, and to a lesser extent, radiation transport from the gas to the solid. In contrast, convective burning involves heat transfer via mass flow. Defects increase the available surface area where combustion can occur and are necessary for convective burning in energetic materials. The effect of defects on combustion has major implications for the safety and reliability of energetic materials.

Voids and cracks in explosives may result from numerous environmental and physical factors. Impact, aging, and variations in temperature and pressure associated with combustion are a few of the factors that can produce defects. At sufficiently high pressures, the surface area of a defect becomes accessible to deflagration. Defects can trap the hot reaction products, creating the necessary pressure gradient for convective burning, and may induce further cracking. A few studies exist on the effects of voids and cracks on the combustion of some common propellants [3,4], but relatively few studies exist of the effects of voids and cracks on the combustion of high

[*] Corresponding author. Tel.: +1-505-665-0380; fax: +1-505-667-0500.
E-mail address: son@lanl.gov (S.F. Son).
[1] Present address: Department of Chemistry, Weber State University, Ogden, UT 84408, USA.

0040-6031/02/$ – see front matter
PII: S0040-6031(01)00802-4

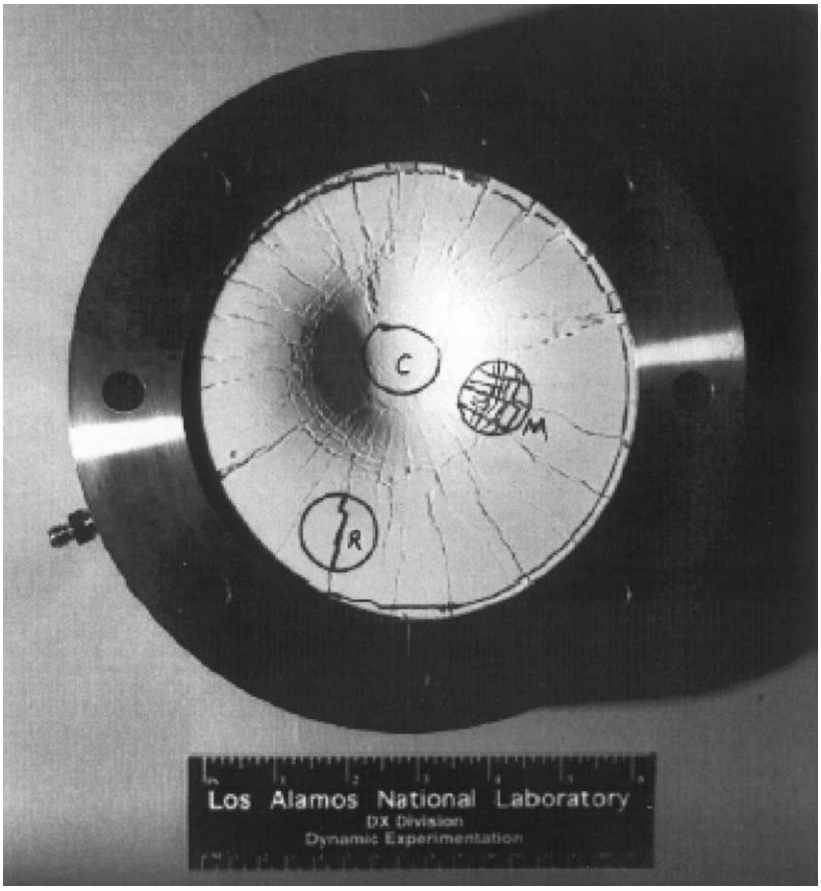

Fig. 1. A PBX 9501 target showing the extensive radial cracking emanated from the impact point that results from low-speed impact by a hemispherical projectile, from Idar et al. [7]. The cover plate has been removed to view the explosive.

explosives (HE) [3]. Ramaswamy and Field have studied hot spot and crack propagation in single crystals of RDX [5]. Formulated explosives, using HMX, (octahydro-1,3,5,7-tetranitro-1,3,5,7-tetrazocine), typically include a binder that makes it possible to desensitize and shape the explosive formulation. Binder affects the number, shape, and size of voids, as well as influences somewhat the combustion [6].

Recent experiments highlight the importance of cracks and voids in the ignition, combustion, and reaction violence of PBX 9501. Fig. 1 shows a PBX 9501 target from a modified Steven Test conducted by Idar et al. [7]. The Steven Test determines the critical impact velocity of a lightly confined energetic material to the low-speed impact of a blunt steel projectile. Radial cracks emanating from the impact point are apparent in Fig. 1 for a test where no sustained reaction occurred. Idar et al. found that damaged PBX 9501 has a significantly lower impact threshold for violent reaction than pristine material.

Henson et al. have conducted shear impact experiments using thin samples of PBX 9501 [8]. A rectangular steel plunger is driven into the lightly confined sample at about 100 m/s. Plunger intrusion causes both shear and non-shear fracturing with reaction initiated along fracture zones as shown in Fig. 2. Skidmore et al. have used microscopy to study damaged samples recovered from the shear impact experiments and find that the HMX along the fracture zones shows clear signs of heating and quenched reaction [9].

Evidence of the importance of crack sustained combustion also appears in elevated-temperature

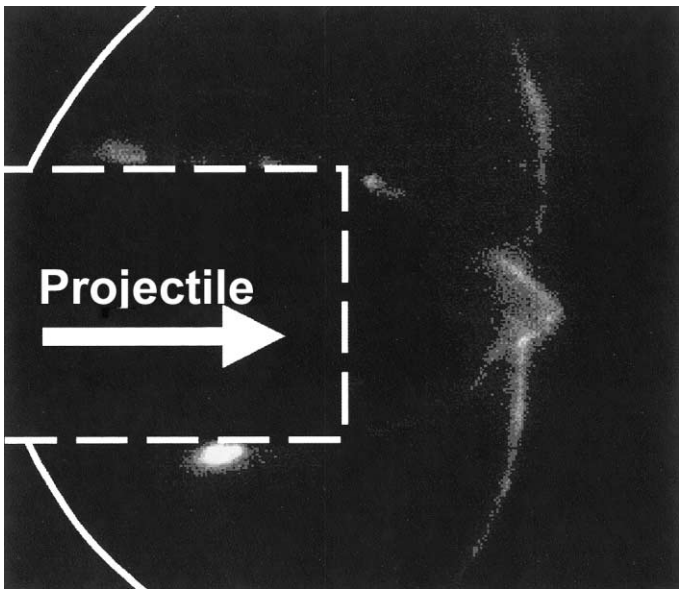

Fig. 2. Ignition of PBX 9501 initiated by shearing-projectile impact from Henson et al. [8]. The dashed box outlines the rectangular plunger that has been driven into the HE from the left. Luminous reaction is seen along the edge of the projectile, in the shear wedge (approximately 2D experiment) in the front of the projectile, and in other stress cracks caused by impact.

experiments, such as the mechanically coupled cook-off (MCCO). Dickson et al. slowly heat a confined sample of PBX 9501 to a well-defined temperature field, then ignite the center of the sample. They detect reaction, indicated by luminous emission, throughout cracks that are caused by pressurization due to production of reactive gases [10]. Fig. 3 shows luminous reaction in cracks during an MCCO experiment. The fast reactive waves, indicated by the luminosity, propagate through the cracks at velocities in the order of 500 m/s.

Precisely machined slots in PBX 9501 allowed us to examine the propagation of fast reactive waves in cracks of PBX 9501, focusing on the reactive wave velocity and on the interplay of pressure and crack size in PBX 9501 [11]. Experiments at initial pressures of 6.0 MPa reveal monotonic reactive wave propagation velocities around 7 m/s for a 100 μm slot. Reactive wave velocities as high as 100 m/s are observed in experiments at initial pressures of 17.2 MPa and various slot widths. Similar experiments at lower pressure exhibit oscillatory reactive wave propagation in the slot with periodic oscillations whose frequencies vary with combustion vessel pressure. Threshold pressure experiments for combustion propagation into closed-end slots of PBX 9501 show that combustion propagates into 2, and 1 mm, and 100, 50, and 25 μm slots at approximately 0.1, 0.2, 0.9, 1.6, and 1.8 MPa, respectively.

Maienschein and Chandler used break wires to study the burn rate of explosives. Visual observations were not made. They report erratic burning at higher pressures in HMX-based explosives with low binder content (∼5 wt.%), but do not observe such erratic burning for similar explosives with greater binder content (15 wt.%) over the range of pressures considered [12]. Similar experiments by Son et al. exhibited erratic burning in high-nitrogen compounds, as indicated by break wires and video. The video records showed that erratic burning results from non-planar reaction propagating into small cracks that were likely present in the sample before they were burned [13]. This observation is consistent with the Maienschein and Chandler experiment where defects and voids are expected to be more predominant in formulations with less binder, leading to erratic burning at higher pressures. Since this erratic burning is non-planar, it cannot be characterized fully by a burning rate. The sample is consumed faster primarily because more burning surfaces are accessed at locally elevated

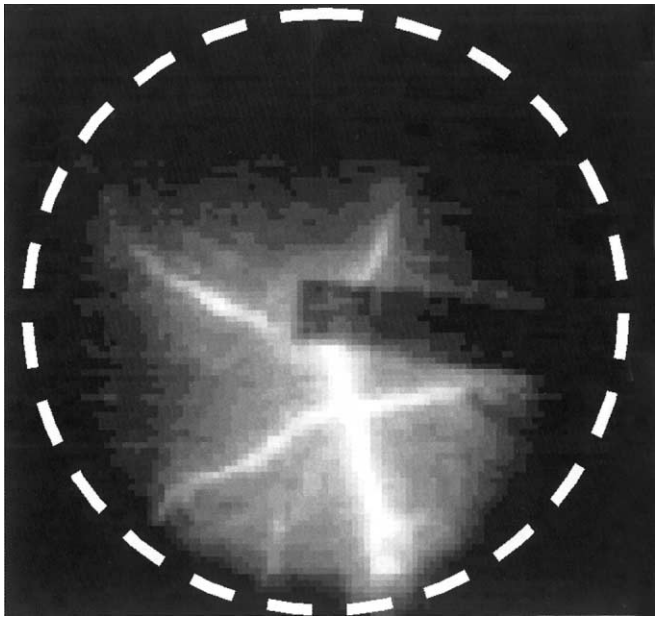

Fig. 3. Luminous reaction in cracks of PBX 9501 during MCCO experiment from Dickson et al. [10]. The dashed circle outlines the disk of HE. The dark rectangular area intruding from the right is a foil sheet used to make contact with a nichrome wire in the center for sample ignition. Ignition of the center of the sample pressurizes the sample causing cracking, and luminous reaction can be seen in these cracks.

pressures, not because the planar burning rate has increased dramatically. Our current efforts examine the effects of thermally and mechanically induced damage on reaction violence in PBX 9501. Our studies investigate the effects of voids and cracks on the combustion of PBX 9501 (HMX with a plasticized Estane binder). In addition to improving our understanding of the safety aspects related to PBX 9501, these experiments provide useful data for ongoing efforts to improve understanding of violent, explosive reactions.

2. Experimental set-up

The material used in this work is PBX 9501. PBX 9501 is a HE formulation composed of 94.9/2.5/2.5/0.1 wt.% of HMX/Estane 5703/1:1 eutectic mixture of bis(2,2-dinitropropyl)acetal (BDNPA) and bis(2,2-dinitropropyl)formal (BDNPF)/diphenylamine (DPA) stablizer or Irganox 1010 free radical inhibitor. A bimodal distribution of 3:1 coarse-to-fine Class 1 and 2 HMX is formulated with the plasticized polymeric binder.

Mechanically damaged samples were obtained from PBX 9501 molding powder that was hydrostatically pressed to an average density of 1.825 g/cm^3 then machined into 0.9525 cm diameter by 1.905 cm long cylindrical pellets. An Instron 5567 Mechanical Testing Workstation with a 30 kN load cell quasi-statically compressed the pellets at constant crosshead speeds of 1.27 or 12.7 cm/min to the point of specimen failure resulting in macrocracking along the shear cones within the specimens and diamond shear cracking patterns on the outer surfaces.

Thermally damaged PBX 9501 samples were prepared by axially pressing molding powder into cylindrical pellets approximately 1 cm tall and 1 cm in diameter with an average density of 1.81 g/cm^3. The pellets are then heated unconfined in a 180 °C oven for 30 min then allowed to cool to room temperature. Nd^{3+}:YAG-laser-based second-harmonic-generation (SHG) and microscopy confirms that heating entirely converts normal β-phase HMX crystals to δ-phase crystals [14].

Microscopic analysis provides an estimate of the extent and characteristics of the damage present in the pellets. Mechanically and thermally damaged samples

were cut along the cylinder axis and vacuum-mounted in low-viscosity epoxy for viewing in cross-section. The specimens were further prepared by polishing with a sequence of fine abrasives for examination by reflected, plane-polarized light. A previous report describes the procedural details [15]. No etching or staining was necessary. Plane-polarized-light microscopy using a Leica DMRXA microscope coupled with a Diagnostic Instruments Spot camera produced digital images of the damage. The spatial resolution of the microscope optics was matched with the camera pixel characteristics to nearly meet the Nyquist limit in each case.

The combustion experiments are performed in a 2 l stainless steel-pressurized combustion vessel. The combustion vessel provides four optical access ports,

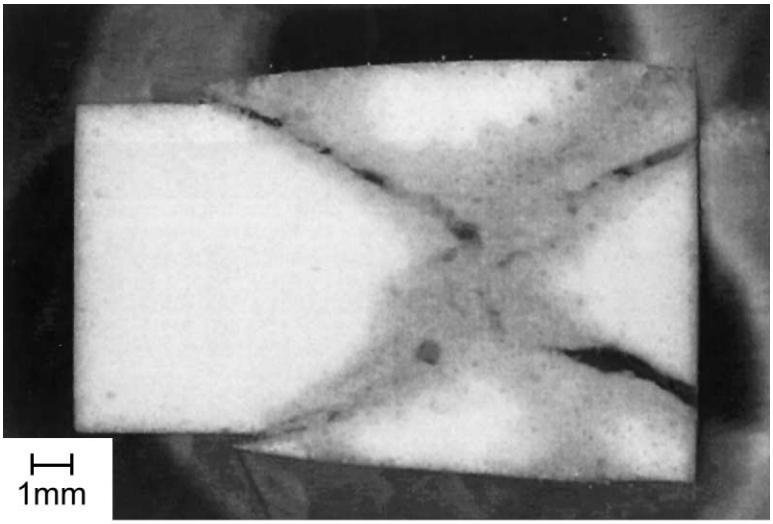

(a)

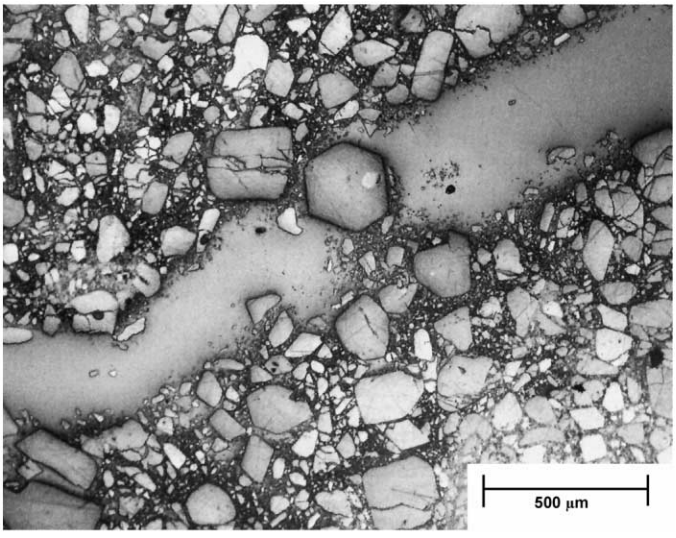

(b)

Fig. 4. Images of a mechanically damaged sample sliced along the cylindrical axis. (a) A low magnification view of the mounted sample. (b) A higher magnification view of the upper-right-hand portion of the sample. (c) A higher magnification view of the central portion of the sample. The original diameter of the pellets was 0.9525 (3/8 in.).

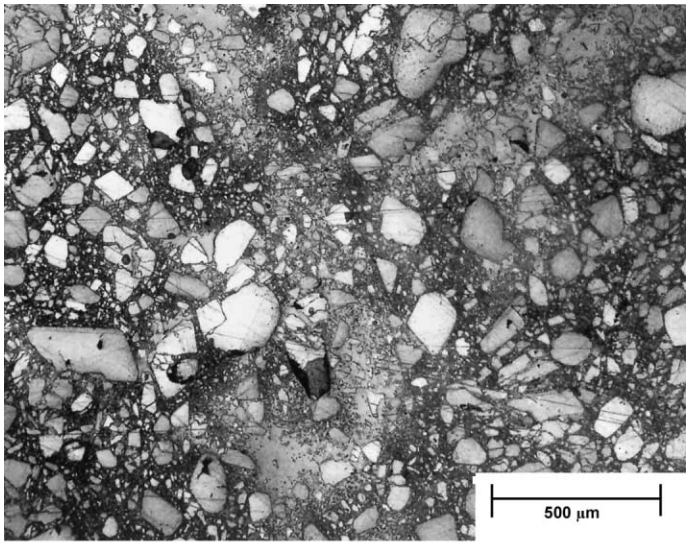

(c)

Fig. 4. (*Continued*).

allowing visual observation of experiments at pressures up to 21 MPa. All experiments are conducted with the pressure vessel and sample initially at room temperature, ∼293 K. Clear epoxy prevents combustion from spreading down the sides of the pellets.

We use several diagnostic tools to monitor combustion. A Canon XL-1 digital video system records the entire experiment at 30 fps and a Red Lake MotionScope PCI 8000S high-speed-video system provides up to 8 s of images at frame rates up to 8000 fps. An Omega Model PX605-10KGI pressure transducer monitors the pressure in the combustion vessel, while the PCB Piezotronics Model 113A23 pressure sensors monitor the transient combustion-vessel pressure and the pressure of the slot relative to the combustion vessel. Tektronix Model TDS 460A and TDS 540A digital oscilloscopes capture the pressure sensor outputs for later storage and analysis.

3. Results and discussion

3.1. Mechanically damaged high explosives

Microscopic studies of mechanically damaged samples reveal extensive cracking and regions of 'rubblization'. Fig. 4 shows images of a mechanically damaged sample sliced along the cylindrical axis. The low magnification view, part (a), shows shear cones, characteristic of compression testing, with large cracks along the margins that form a large 'X'. Higher magnification views, parts (b) and (c), show details of the upper right hand leg of the 'X' and the central region of extensive damage where the shear cones approach, respectively. The average large crack width is about 200 μm though some areas are wider while other areas appear to be nearly blocked as shown in Fig. 4. Near the center of the pellet where the shear cones merge, fine debris replaces the large cracks visible. The connected porosity in this region is sufficient to allow the mounting epoxy to flow into it, resulting in the darkening that is apparent around the shear cones. The epoxy does not enter and darken the regions away from the margins of the shear cones where little damage has occurred.

Combustion experiments were designed to observe the reaction of mechanically damaged pellets at a series of pressures to determine the threshold pressure necessary to produce violent reaction. Fig. 5 presents a sequence of images showing the combustion of a mechanically damaged sample and Fig. 6 plots combustion vessel pressure versus time for the image sequence. The sample is ignited on the left and deflagration progresses to the right. The first frame

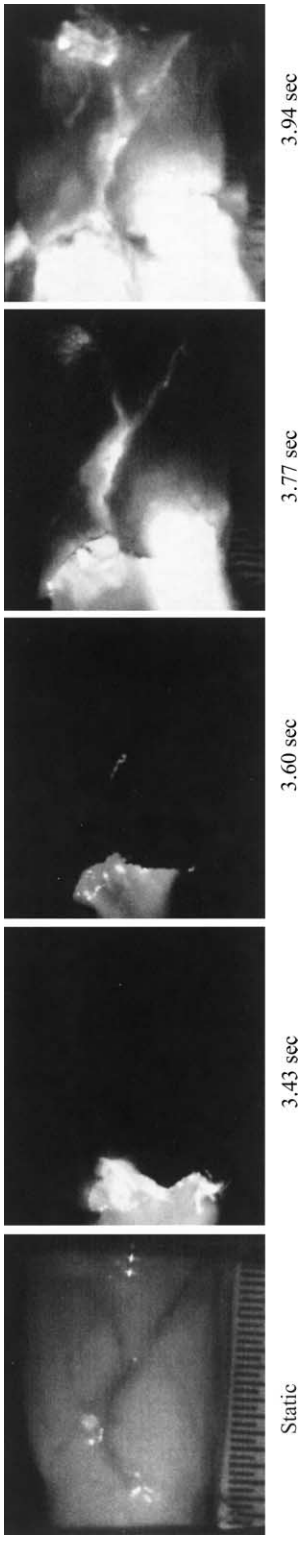

Fig. 5. This sequence of images shows the combustion of a mechanically damaged sample.

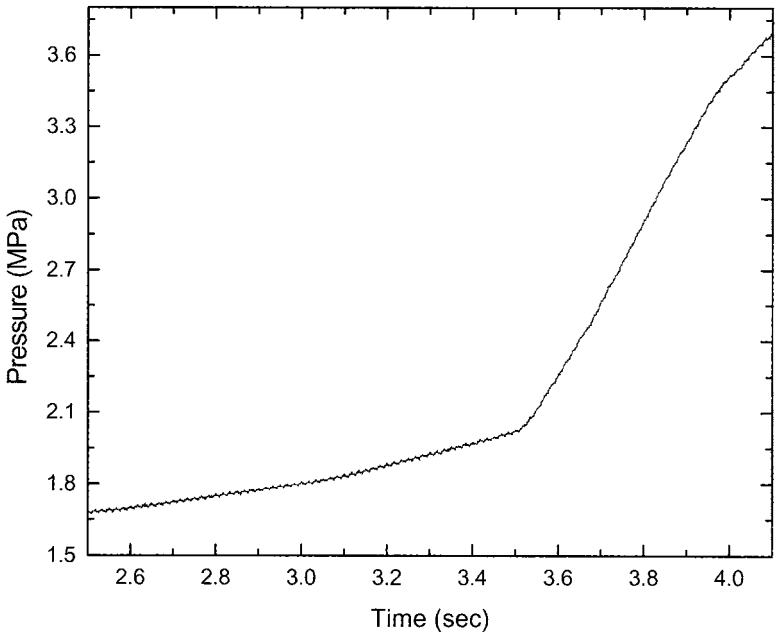

Fig. 6. Plot of pressure vs. time for combustion of a mechanically damaged sample.

shows the sample prior to the experiment. The second frame shows normal burning following sample ignition, with the damage appearing to affect the curvature. The third frame shows luminous reaction in a crack ahead of the normally burning surface, the fourth frame shows more intense reaction accessing additional cracks, and the fifth frame shows the entire pellet being consumed in the reaction. Combustion

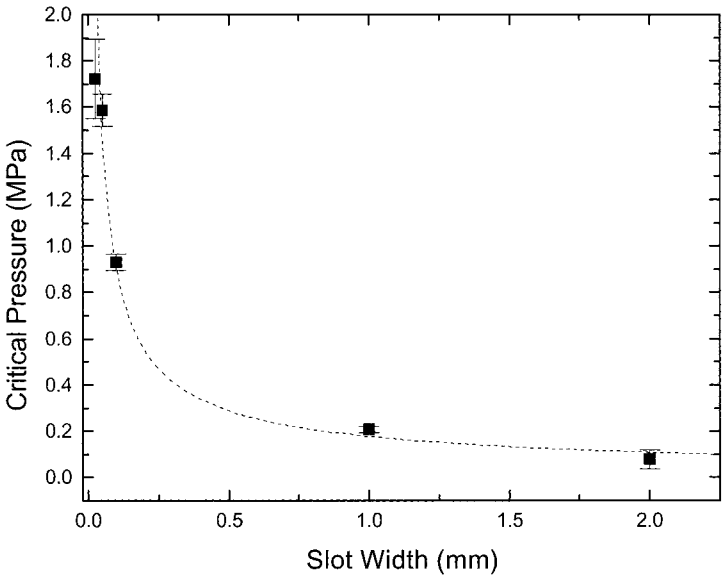

Fig. 7. Plot of critical pressure vs. slot width for PBX 9501.

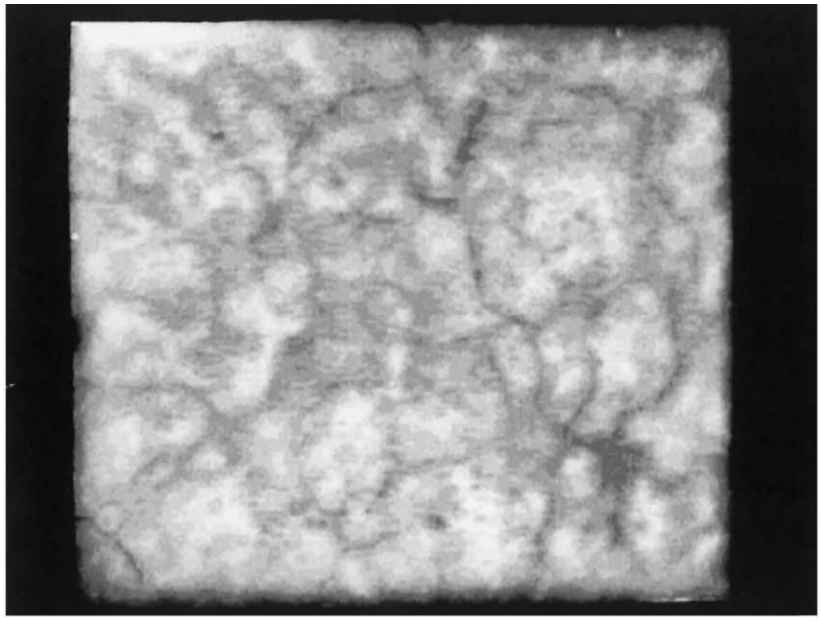

(a)

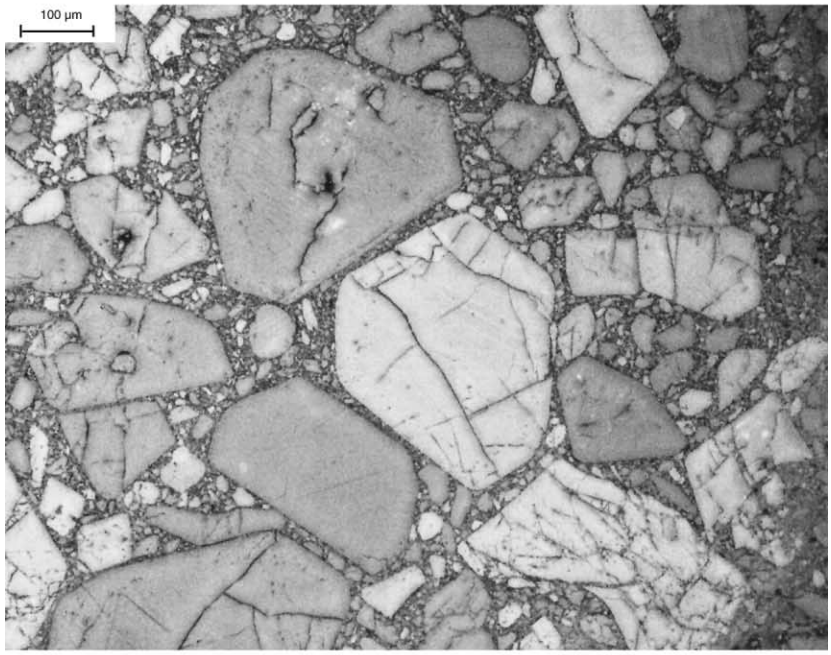

(b)

Fig. 8. Images for the thermal-damaged sample sliced along the cylindrical axis. (a) A low magnification view of the mounted sample. (b) Higher-magnification view of a pristine PBX 9501 sample. (c) A higher-magnification view of a sample that has been heated in an oven at 180 °C for 30 min.

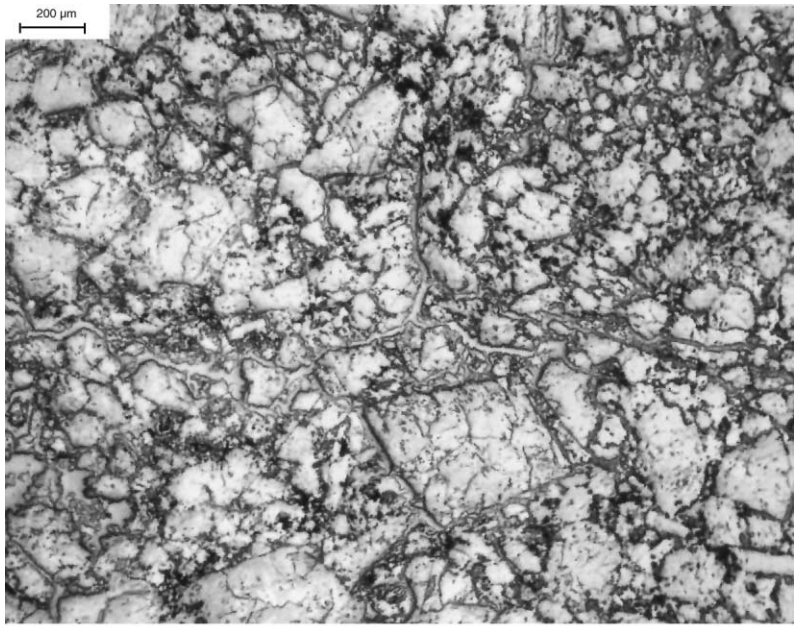

(c)

Fig. 8. (*Continued*).

vessel pressure climbs gradually during the period of normal burning then rises rapidly when convective combustion enters and begins to consume the voids in the pellet.

A critical pressure for violent reaction of the mechanically damaged samples is observed at 1.4 ± 0.6 MPa. Below this pressure, damaged pellets burn in a normal, planar manner, while above this pressure, reaction enters the cracks and voids in the pellet, resulting in violent, convective burning. The plot in Fig. 7 displays the results of the previously reported critical pressure measurements for reaction entering machined-closed-end slots in PBX 9501 [13]. A simplified theoretical expression proposed by Belyaev et al. describes the interdependence of the critical pressure and the slot width [3]

$$p_c^{1+2n} w^2 = \text{constant}, \quad (1)$$

where p_c is the critical pressure, n the conductive burn rate pressure exponent and w the slot width. The dashed line in Fig. 7 results from Eq. (1) where we have assumed n to equal 0.92, the value for PBX 9501 [13], and the constant equal to 8×10^8 in SI units. The critical pressure for violent reaction in our current results suggest that the mechanically damaged samples have an effective defect and crack width of about 25 μm. Effective defect dimensions determined from our critical-pressure experiments are much smaller than the ~200 μm cracks along the shear cone margins observed by microscopy. This is probably because the narrowest passage in the cracks must be accessed by the flame before convective burning can be fully established. In other words, the fine scale connected porosity of the damage appears to control the spread of the flame into the crack. Furthermore, the surface area of the large macrocracks is much less than the surface area of the fine scale damage that is only accessible at higher pressures. Truly violent reaction occurs when the pressure allows burning to occur in the debris region around the large cracks and in the center of the pellet. The large cracks provide access for combustion to reach the porous debris regions but do not contribute much to reaction violence.

3.2. Thermally damaged high explosives

Microscopic studies of thermally damaged samples reveal extensive cracking uniformly distributed

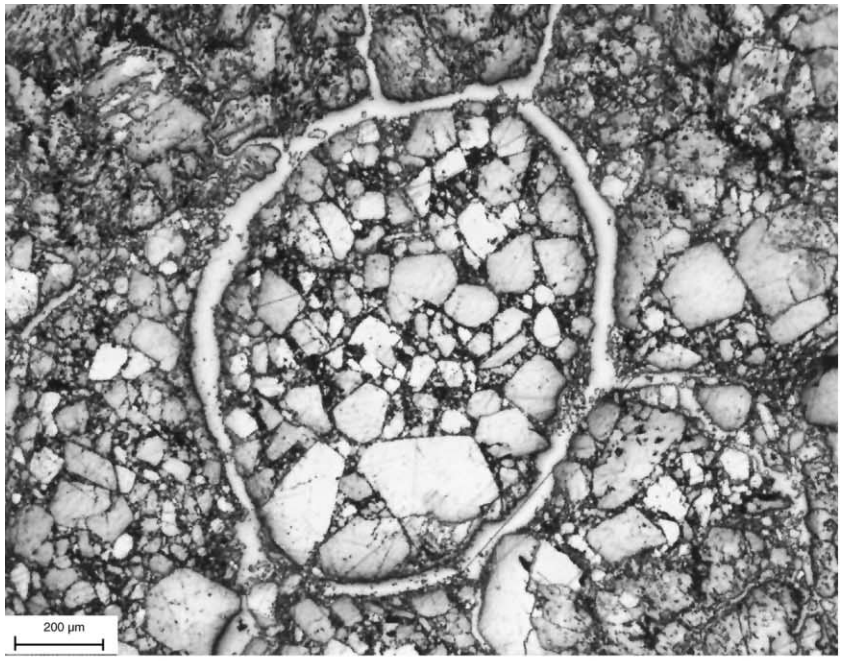

(a)

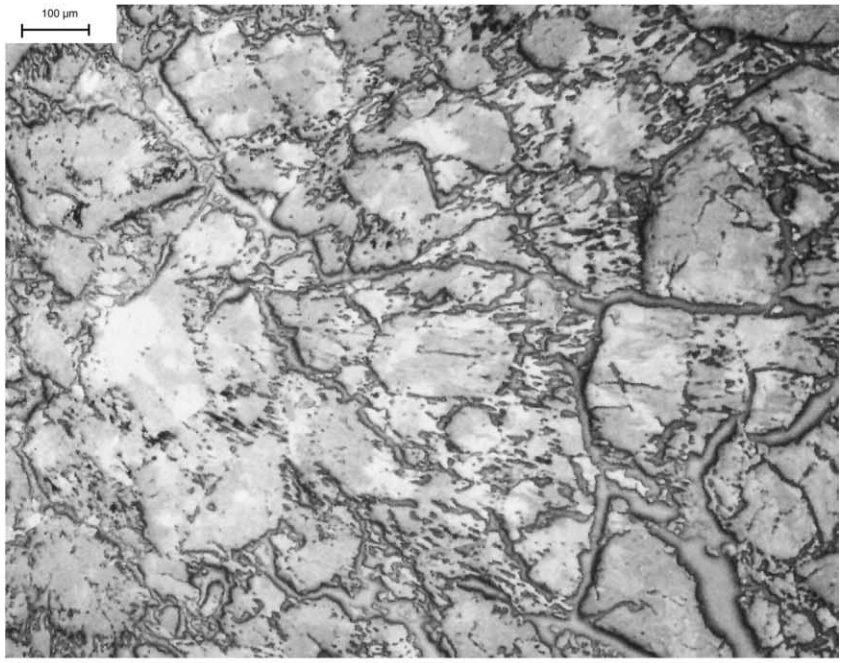

(b)

Fig. 9. This figure shows sectioned pellets that were heated at 180 °C for (a) 15 min, and (b) 30 min.

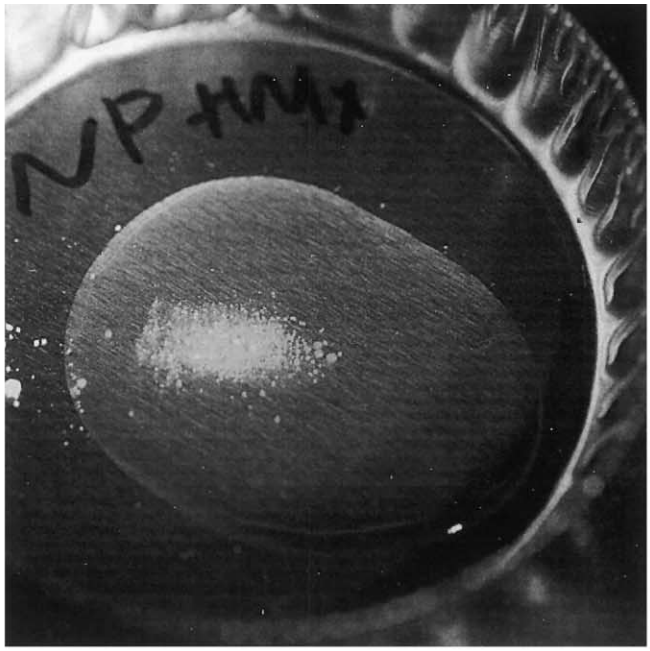

(a)

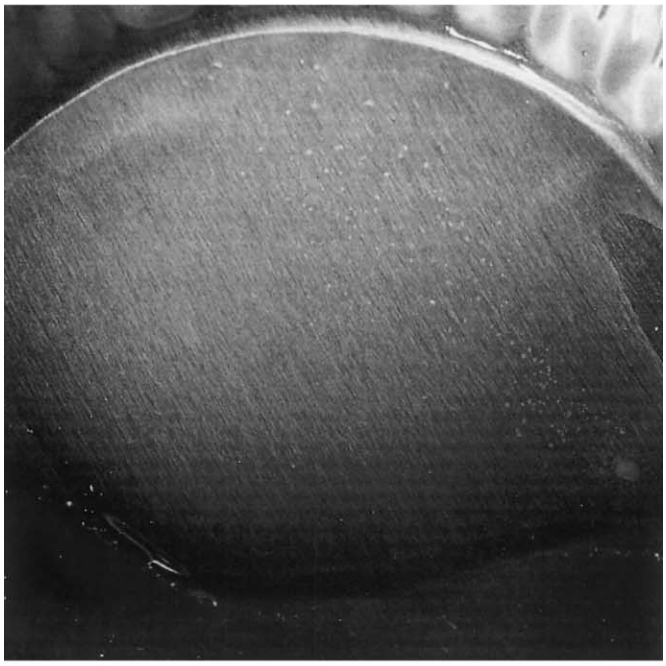

(b)

Fig. 10. This figure shows HMX crystals suspended in BDNPA/BDNPF plasticizer. In (a), suspended crystals are shown before heating. (b) The solution after heating. The crystals in the plasticizer during heating were dissolved. (c) A microscopic picture of a solution similar to (a) placed on a slide at room temperature. (d) Recrystallization that was observed after heating followed by cooling.

(c)

Fig. 10. (*Continued*).

throughout the pellet. Fig. 8 shows images of a thermally damaged sample sliced along the cylindrical axis. The low magnification view, part (a), shows the uniformly distributed nature of the thermal damage. The higher magnification views, parts (b) and (c), compare a pellet that has not been heated, left, with one that has been heated in a 180 °C oven for 30 min, respectively. Individual HMX crystals and binder regions, which are clearly identifiable in the unheated sample, are difficult to identify in the heated samples. Part (b) of Fig. 9 shows another section of the heated sample at even higher magnification. Large, 2–20 μm cracks are randomly distributed throughout the heat-treated sample, but are not observed in the unheated sample. Nd^{3+}:YAG-laser-based SHG and microscopy confirms that heating entirely converts the normal β-phase HMX crystals to δ-phase crystals [14]. Expansion due to heating and the β–δ-phase transition changes the crystalline structure and produces fractures and voids throughout the pellets. The heated pellets have a density that has been reduced to 1.53 g/cm^3, compared with a pristine density of 1.81 g/cm^3.

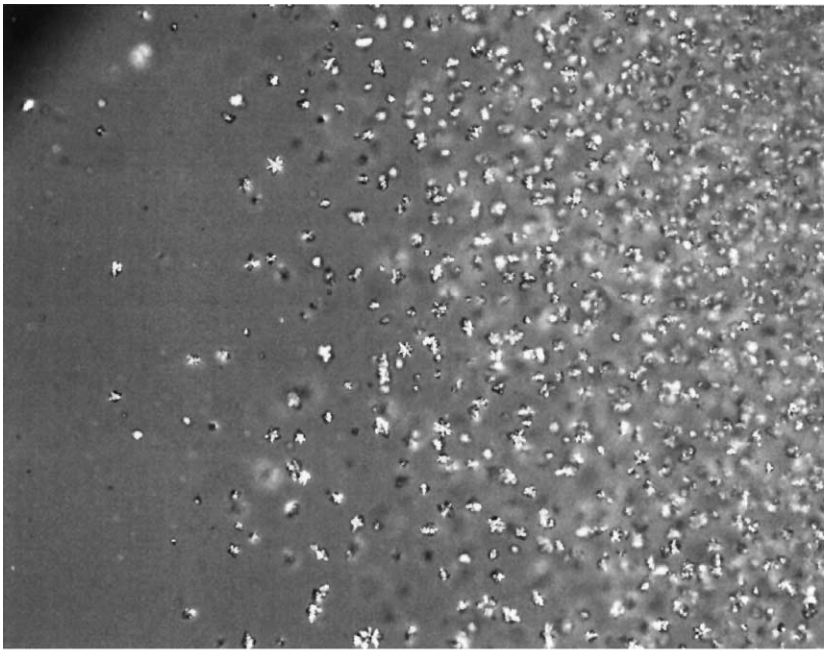

(d)

Fig. 10. (*Continued*).

The mass loss is about 0.7% of the 1.3 g pristine pellets. The very small crystals, present in the binder between the large crystals in the unheated sample, are not observed after heating, and the large areas of HMX no longer have sharp crystalline faces. This may be caused by solvation of HMX crystals in the binder during heating, followed by some recrystalization during cooling. This change in morphology was unanticipated. Consequently, we examined this process further.

Additional identical pellets were heated for only 15 min, cooled and then examined. The resulting density was 1.56 g/cm^3. Examining this sample we observed that most of the sample appears similar to the sample heated for 30 min (see part (c) of Fig. 8 and part (b) of Fig. 9), except for pockets of material that does not appear to have converted to δ-phase material or affected by solvation (see Fig. 9). Small areas of pristine-like material were distributed throughout the sample, rather than concentrated in the center or near the edges as might be expected. In these ''unaffected'' areas, faceted edges of crystals are observed and fine particles are observed (similar to part (a) of Fig. 8). In heat-affected areas the crystals are more opaque due to microcracks (indicative of β–δ-phase transition), small crystals appear to have been dissolved, and faceted edges are not clearly observed.

We also examined the heating of the binder constituents (Estane and BDNPA-F plasticizer) alone and in contact with HMX. BDNPA-F plasticizer with a small amount of HMX powder, or by itself, lost about 2% of its mass when heated in an oven in air held at 180 °C for 30 min. In contrast, Estane (without BDNPA-F) lost only about 0.05% in weight. The percent weight loss of the Estane-based binder (Estane and BDNPA-F) was about 1% under the same conditions. Fig. 10 shows the BDNPA-F plasticizer with a small amount of HMX powder added. At room temperature the HMX is affected very little, as can be seen in parts (a) and (c) of Fig. 10. Upon heating, the particles suspended in the plasticizer dissolve (see part (b) of Fig. 10). After cooling, tiny crystals were observed recrystallizing from the solution (see part (d) of Fig. 10). Sprinkling a small amount of HMX powder on a piece of Estane-based binder and heating the sample also resulted in indications of dissolving and recrystalization (see Fig. 11). Bubbles were also observed in the binder, as shown in Fig. 11. HMX in contact with Estane showed some softening of the

Estane, but no indications of solvation of the HMX. These results indicate that the BDNPA-F plasticizer is responsible for the solvation of the HMX in PBX 9501. Published solubility data of HMX in BDNPA-F plasticizer at these elevated temperatures is not available. Some unpublished data indicates that between 25 and 120 °C, the solubility ranges from 0.05 to 1.16 g/100 ml solution. This would not seem to be high enough (even extrapolated to 180 °C) to account for the significant morphology change observed in heated PBX 9501. However, when a slight supersaturation is obtained in a solution by dissolving extremely fine particles of crystalline material in the mother liquor, held at constant temperature large crystals will grow still larger via the diminution or disappearance of the small ones in contact with the same mother liquor. This phenomenon is known as Ostwald ripening [16]. Consequently, it is possible that at elevated temperature the fine particles are dissolved by the BDNPA-F and then continually recrystallize onto the large particles. The solubility of HMX in BDNPA-F plasticizer should be measured in this temperature range in future work. The observation that fine particles are not observed upon heating PBX 9501 may have implications for cookoff modeling.

Combustion experiments of thermally damaged pellets at a series of pressures were performed to determine the threshold pressure necessary to produce violent reaction. Fig. 12 is a sequence of images showing the combustion of a thermally damaged sample. The sample is ignited on the left and deflagration progresses to the right. The first frame shows the sample prior to the experiment. The second frame shows normal burning following sample ignition. The third frame shows luminous reaction in a crack ahead of the normally burning surface and the fourth frame shows brighter reaction in the crack as reaction progresses and the surface of the crack regresses.

Fig. 11. This figure shows HMX crystals poured on a piece of Estane-based binder. In (a), the binder and HMX are shown before heating. In (b), the sample is shown after heating.

(b)

Fig. 11. (*Continued*).

Analogous to the mechanically damaged samples, the combustion vessel pressure climbs gradually during the period of normal burning then rises rapidly when convective combustion enters and begins to consume the voids in the pellet.

A critical pressure for violent reaction of our thermally damaged samples is observed at 9.2 ± 0.4 MPa. Below this pressure, damaged pellets burn in a normal, planar manner, while above this pressure, reaction enters the cracks and voids in the pellet, resulting in violent, convective burning. Convective burning was observed in 10 thermally damaged samples. A planar front was *never* observed during these violent burns. This has significant modeling implications.

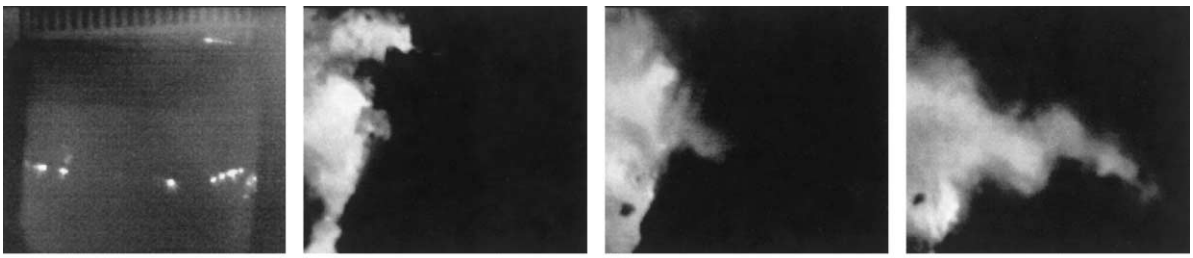

Static 1.71 sec 1.80 sec 1.89 sec

Fig. 12. This sequence of images shows the combustion of a thermally damaged pellet.

Following the same analysis as for the mechanically damaged samples, the critical pressure for violent reaction in our current results suggest that the thermally damaged samples have an effective defect and crack width of about 4 μm. This is in the low end of the range of the microscopically observed damage noted above. Again, the smaller widths of the crack appear to control the onset to convective burning. Additionally, below the threshold for violent reaction, we find that the normal burn rate and pressure exponent of the heat-damaged samples are similar (within about 10%) to those for undamaged samples.

4. Conclusions

Mechanically damaged samples, damaged by quasi-static pressing, exhibit large, 200–300 μm stress fractures accompanied by extensive rubblization. Combustion experiments determine a 1.4 ± 0.6 MPa critical pressure for the onset of violent convective combustion, consistent with 25 μm connected porosity. Thermally damaged samples, damaged by heating in a 180 °C oven for 30 min, exhibit 2–20 μm randomly distributed cracking. The fine HMX particles are not observed in the heated samples and clear facets are not observed on the larger crystals. A solvation process appears to have occurred. Results presented in this paper indicate that the BDNPA-F plasticizer is responsible for the solvation of the HMX in PBX 9501 at elevated temperatures. Combustion experiments show at 9.2 ± 0.4 MPa critical pressure for the onset of violent convective combustion, consistent with connected porosity of 4 μm. The smaller length-scales of the connected porosity appear to control the onset of convective burning. In even the thermally damaged material, which has quite uniformly distributed damage, convective burning is observed to propagate in a very non-planar fashion. These results have implications to modeling efforts. The burn rate and pressure exponent of thermally damaged PBX 9501 are similar to those of the pristine material below the critical pressure. Future work should include combustion driven cracks and the combustion of partially decomposed materials, as well as more quantitative measurement of the crack size distribution and surface area.

Acknowledgements

We acknowledge the support of Los Alamos National Laboratory, under contract W-7405-ENG-36. In particular, we acknowledge the support of the Laboratory Directed Research and Development Program of Los Alamos National Laboratory.

References

[1] B.W. Asay, S.F. Son, J.B. Bdzil, Int. J. Multiphase Flow 22 (1996) 923.
[2] A.F. Belyaev, V.K. Bobolev, Transition from Deflagration to Detonation in Condensed Phases, 1975, (National Technical Information Service, Springfield, VA, Trans.; original work published in 1973).
[3] H.H. Bradley, T.L. Boggs, Convective Burning in Propellant Defects: A Literature Review, Naval Weapons Center, China Lake, CA Report No. NWC-TP-6007, 1978.
[4] M. Kumar, K.K. Kuo, in: K. Kuo, M. Summerfield (Eds.), Fundamentals of Solid Propellant Combustion, Vol. 90, AIAA, Inc., New York, 1984, pp. 339–350.
[5] A.L. Ramaswamy, J.E. Field, J. Appl. Phys. 79 (1996) 3842.
[6] S.F. Son, H.L. Berghout, C.A. Bolme, et al., Proc. Int. Symp. Combustion 28 (2000) 919.
[7] D.J. Idar, R.A. Lucht, J.W. Straight, et al., in: Proceedings of the 11th International Detonation Symposium, Snowmass, CO, 1998, pp. 101–110.
[8] B.F. Henson, B.W. Asay, P.M. Dickson, et al., in: Proceedings of the 11th International Detonation Symposium, Snowmass, CO, 1998, pp. 325–331.
[9] C.B. Skidmore, D.S. Phillips, B.W Asay, et al., Shock Compression of Condensed Matter, American Institute of Physics, Snowbird, UT, 1999, pp. 659–662.
[10] P.M. Dickson, B.W. Asay, B.F. Henson, et al., in: Proceedings of the 11th International Detonation Symposium, Snowmass, CO, 1998, pp. 606–611.
[11] H.L. Berghout, S.F. Son, B.W. Asay, in: Proceedings of the JANNAF PSHS Meeting, Cocoa Beach, FL, 1999.
[12] J.L. Maienschein, J.B. Chandler, in: Proceedings of the 11th International Detonation Symposium, Snow Mass, CO, 1998, pp. 872–879.
[13] S.F. Son, H.L. Berghout, C.A. Bolme, et al., in: Proceedings of the JANNAF PSHS Meeting, Cocoa Beach, FL, 1999.
[14] B.F. Henson, B.W. Asay, R.K. Sander, et al., Phys. Rev. Lett. 82 (1999) 1213.
[15] C.B. Skidmore, D.S. Phillips, N.B. Crane, Microscope 45 (1997) 127.
[16] A. Weissberger, Technique of Organic Chemistry, Vol. III, Part I, Crystallization and Recrystallization, Interscience Publishers, 1956 (Chapter III).